Commun. Comput. Phys.
doi: 10.4208/cicp.180411.090112a

Vol. **12**, No. 5, pp. 1392-1416
November 2012

Numerical Solutions of Coupled Nonlinear Schrödinger Equations by Orthogonal Spline Collocation Method

Qing-Jiang Meng[1,*], Li-Ping Yin[2], Xiao-Qing Jin[1] and Fang-Li Qiao[3]

[1] *Department of Mathematics, University of Macau, Macao.*
[2] *First Institute of Oceanography, State Oceanic Administration, Qingdao, Shandong 266061, China & College of Physical and Environmental Ocanography, Ocean University of China, Qingdao, Shandong 266003, China.*
[3] *Key Laboratory of Marine Science and Numerical Modeling of State Oceanic Administration & First Institute of Oceanography, State Oceanic Administration, Qingdao, Shandong 266061, China.*

Received 18 April 2011; Accepted (in revised version) 9 January 2012

Available online 8 May 2012

Abstract. In this paper, we present the use of the orthogonal spline collocation method for the semi-discretization scheme of the one-dimensional coupled nonlinear Schrödinger equations. This method uses the Hermite basis functions, by which physical quantities are approximated with their values and derivatives associated with Gaussian points. The convergence rate with order $\mathcal{O}(h^4+\tau^2)$ and the stability of the scheme are proved. Conservation properties are shown in both theory and practice. Extensive numerical experiments are presented to validate the numerical study under consideration.

AMS subject classifications: 65N35, 35C45, 35L65

Key words: Coupled nonlinear Schrödinger equations, orthogonal spline collocation method, conservation law.

1 Introduction

The coupled nonlinear Schrödinger (CNLS) equations were first derived 30 years ago by Benney and Newell [6] for two interacting nonlinear packets in dispersive and conservative systems. Since then, the CNLS equations have been appeared in a great variety of physical situations. Its applications can be found in many areas of physics, including nonlinear optics and plasma physics, see, e.g., [1, 16, 22, 24, 28]. These equations also

*Corresponding author. *Email addresses:* qjmeng04@163.com (Q.-J. Meng), lipyconstance@163.com (L.-P. Yin), xqjin@umac.mo (X.-Q. Jin), qiaofl@fio.org.cn (F.-L. Qiao)

model a beam propagation inside crystals or photorefractives as well as water wave interactions. In this paper, we consider the following CNLS equations:

$$\mathbf{i}\frac{\partial\varphi}{\partial t}+\frac{\partial^2\varphi}{\partial x^2}+(|\varphi|^2+\beta|\psi|^2)\varphi=0, \tag{1.1a}$$

$$\mathbf{i}\frac{\partial\psi}{\partial t}+\frac{\partial^2\psi}{\partial x^2}+(|\psi|^2+\beta|\varphi|^2)\psi=0, \tag{1.1b}$$

where φ and ψ represent complex amplitudes of two polarization components, β is a real-valued cross-phase modulation coefficient, $\mathbf{i}=\sqrt{-1}$, x is the space variable and t is the time variable. If $\beta=0$, Eq. (1.1) becomes two copies of a single nonlinear Schrödinger equation which is integrable; when $\beta=1$, Eq. (1.1) is known as the Manakov system which is also integrable. In all the other cases, the situations are much more complicated from different viewpoints. These equations have been studied intensively in the past 10 years [8, 14, 18]. Much work has been done on collisions in a large array of physical systems. Various collision scenarios, such as transmission, reflection, annihilation, trapping, creation of solitary waves and even mutual spiraling, have been reported.

There are a great deal of numerical methods used to solve the CNLS equations. Antoine et al. [2] give a review to discuss different techniques to solve numerically the time-dependent Schrödinger equation on unbounded domains. Klein et al. [15] propose a hierarchy of novel absorbing boundary conditions for the one-dimensional stationary Schrödinger equation with general potential. The time-splitting spectral method for solving a general model of wave optical interactions is obtained by Bao et al. [3–5,30]. Xu and Shu [25–27] develop local discontinuous Galerkin methods for solving high-order time-dependent partial differential equations including CNLS equations. Ismail and Taha [14] introduce a finite difference method for the numerical simulation of the CNLS equations. The multi-symplectic splitting method is proposed to solve the CNLS equations in [9] and the constrained interpolation profile-basis set method is considered in [21]. Wang [23] presents a numerical solution of the single and coupled nonlinear Schrödinger equations using a split-step finite difference method. However, in these numerical simulations and computations, many constraints are required in order to keep the accuracy and stability. Moreover, many properties of the system, such as energy conservation and momentum conservation, are neglected.

The purpose of this paper is to investigate the use of the orthogonal spline collocation (OSC) method with the piecewise Hermite cubic polynomials for the spatial discretization of Eq. (1.1). This method has evolved as a valuable technique for the solution of many types of partial differential equations; see [11] for a comprehensive survey. The popularity of such a method is in part to its conceptual simplicity and ease of implementation. Another attractive feature of the OSC method is their superconvergence. One obvious advantage of the OSC method over the finite element method is that the calculation of the coefficient matrices is very efficient since no integral calculation is required. Another advantage of this method is that it systematically incorporates boundary conditions and interface conditions. In comparison with finite difference methods, spline

collocation method provides approximations to the solution and its derivative with respect to x at all points in the domain of problems. In this paper, we present the use of the OSC method for the semi-discretization scheme of the one-dimensional coupled nonlinear Schrödinger equations. This method uses the Hermite basis functions, by which physical quantities are approximated with their values and derivatives associated with Gaussian points. The accuracy and stability of solutions with order $\mathcal{O}(h^4+\tau^2)$ are verified by ensuring that conserved quantities remain almost constant, where h and τ denote the spatial and temporal mesh sizes respectively. It has been shown that the scheme has remarkable mass, momentum and energy conserved properties.

The paper is organized as follows. In Section 2, we briefly review the OSC method and give the discretization scheme of the CNLS equations. In Section 3, we present conserved quantities of the scheme. In Section 4, we demonstrate the accuracy and stability of the scheme. Numerical tests with various initial conditions of the CNLS equations like single soliton, interaction of two solitons, interaction of arbitrary initial conditions and periodic boundary conditions are reported in Section 5. Finally, in Section 6 we end our paper with some remarks.

2 The OSC method for CNLS equations

2.1 Preliminaries

The OSC method with piecewise polynomials of arbitrary degree for solving two-point boundary value problems is introduced and analyzed in [7]. The analysis of [7, 10] includes proofs of the superconvergence of the OSC approximations on nonuniform partitions. To describe the OSC method, we introduce some notations.

For a given complex-valued function φ, we denote the complex conjugate of φ by $\bar{\varphi}$. Given any space S of functions, let $\mathcal{R}(S)$ denote the set of all real-valued functions in S. Throughout the paper, we use C to denote a generic positive constant and make repeated use of the inequality

$$de \le \varepsilon d^2 + \frac{1}{4\varepsilon}e^2, \qquad \varepsilon \ge 0, \qquad d,e \in \mathbb{R},$$

without explicit mention each time.

With a positive integer N, given a partition of $\overline{\Omega}=[x_L,x_R]$

$$\Delta: \ x_L = x_0 < x_1 < \cdots < x_N = x_R.$$

Let $h_j = x_j - x_{j-1}$, $j=1,2,\cdots,N$ and $h=\max_{1\le j\le N} h_j$. A family $\mathcal{F}$ of partitions is said to be quasi-uniform if there exists a finite positive number σ such that

$$\max_{1\le j\le N} \frac{h}{h_j} \le \sigma$$

for every partition Δ in $\mathcal{F}$ [17]. We assume that the partition Δ is a member of a quasi-uniform family. Let $\{t_n\}_{n=0}^J$ be a partition of $[0,T]$, where $t_n=n\tau$ and $\tau=T/J$. In the paper, h and τ denote the spatial and temporal mesh sizes respectively.

Let $\mathcal{M}^0$ be the space of piecewise Hermite cubics on Ω defined by

$$\mathcal{M}^0(\Delta)=\Big\{v|v\in C^1(\overline{\Omega}):v|_{[x_{j-1},x_j]}\in\mathcal{P}_3 \text{ and } v(x_L)=v(x_R)=0\Big\},$$

where $\mathcal{P}_3$ denotes the set of all polynomials of degree less than or equal to 3.

Let $\{\lambda_k\}_{k=1}^2$ denote the roots of the Legendre Polynomial of degree 2, where $\lambda_1\equiv(1-1/\sqrt{3})/2$ and $\lambda_2\equiv(1+1/\sqrt{3})/2$. These are the nodes of the 2-point Gaussian quadrature rule on the interval Ω with corresponding weights $\omega_k=1$ for $k=1,2$. To apply the collocation method, we introduce collocation points $\mathcal{G}=\{\xi_{j,k}\}_{j,k=1}^{N,2}$ taken as

$$\xi_{j,k}=x_{j-1}+h_j\lambda_k,\quad j=1,2,\cdots,N,\quad k=1,2.$$

For $\varphi,\psi\in C^1(\bar{\Omega})$, we define a discrete inner product and its induced norm by

$$\langle\varphi,\psi\rangle_{\mathcal{G}}=\sum_{j=1}^N h_j\sum_{k=1}^2\omega_k\varphi(\xi_{j,k})\bar{\psi}(\xi_{j,k}),\qquad \|\varphi\|_{\mathcal{G}}=\langle\varphi,\varphi\rangle_{\mathcal{G}}^{\frac{1}{2}}.$$

We always use the following difference quotient notations:

$$(\varphi_j^n)_t=\frac{\varphi_j^{n+1}-\varphi_j^n}{\tau},\qquad \varphi_j^{n+\frac{1}{2}}=\frac{1}{2}(\varphi_j^{n+1}+\varphi_j^n),\qquad (\varphi_j^n)_{xx}=\frac{\varphi_{j+1}^n-2\varphi_j^n+\varphi_{j-1}^n}{h^2}.$$

Let r be a nonnegative integer and denote by

$$\|\varphi\|_{H^r(\Omega)}=\Big(\sum_{j=0}^r\Big\|\frac{\partial^j\varphi}{\partial x^j}\Big\|_{L^2(\Omega)}^2\Big)^{\frac{1}{2}},$$

the norm on the usual Sobolev space $H^r(\Omega)$. We denote by $L^s(0,T;H^{r+3}(\Omega))$ the Banach space of all L^s integrable functions from $(0,T)$ into $H^{r+3}(\Omega)$ with norm

$$\|\varphi\|_{L^s(0,T;H^{r+3}(\Omega))}=\Big(\int_0^T\|\varphi\|_{H^{r+3}(\Omega)}^s dt\Big)^{\frac{1}{s}}$$

for $s\in[1,+\infty)$ and the standard modification for $s=+\infty$. In this paper, we take $r=3$.

Since Δ belongs to a quasi-uniform family of partitions, it can be shown using results of [10] that there exist positive constants C_1 and C_2 such that for any $\varphi\in\mathcal{M}^0(\Delta)$,

$$C_1\|\varphi\|_{\mathcal{G}}\le\|\varphi\|_{L^2(\Omega)}\le C_2\|\varphi\|_{\mathcal{G}}. \tag{2.1}$$

We now use the Hermite basis functions where it is easy to define φ_h^n and ψ_h^n at the collocation points. Recently, restricting problems to a bounded domain, the Fourier spectral

methods are applicable, see Zhang et al. [30]. In the present situation, for any time integration method, the number of basis functions required for the Hermite spectral method is always smaller than the number of basis functions required for the Fourier spectral method, see [20] for details. Let $\{\phi_j^n\}_{j=1}^{2N}$ be basis functions of $\mathcal{M}^0(\Delta)$, so one may write

$$\varphi_h^n(x)=\sum_{j=1}^{2N}\hat{\varphi}_j^n\phi_j^n(x),\quad \psi_h^n(x)=\sum_{j=1}^{2N}\hat{\psi}_j^n\phi_j^n(x),\quad n=0,1,2,\cdots,J-1, \tag{2.2}$$

where $\hat{\varphi}_j^n$, $\hat{\psi}_j^n$ $(j=1,2,\cdots,2N;\ n=0,1,2,\cdots,J-1)$ are unknown coefficients which should be worked out.

We introduce the following lemmas.

Lemma 2.1. (see [10,17]) *For $\varphi,\psi\in\mathcal{R}(\mathcal{M}^0(\Delta))$, we have*

$$\langle\varphi_x,\psi\rangle_{\mathcal{G}}=-\langle\psi_x,\varphi\rangle_{\mathcal{G}},\qquad -\langle\varphi_{xx},\psi\rangle_{\mathcal{G}}=-\langle\varphi,\psi_{xx}\rangle_{\mathcal{G}}, \tag{2.3}$$

$$-\langle\varphi_{xx},\varphi\rangle_{\mathcal{G}}\geq\|\varphi_x\|_{L^2(\Omega)}. \tag{2.4}$$

Lemma 2.2. (Discrete Gronwall inequality, see [12]) Let $\omega(k)$ and $\rho(k)$ be nonnegative grid functions. If $C>0$, $\rho(k)$ is nondecreasing and

$$\omega(k)\leq\rho(k)+C\tau\sum_{l=0}^{k-1}\omega(l),$$

then for any $0\leq k\leq N$, we have

$$\omega(k)\leq\rho(k)e^{Ck\tau}. \tag{2.5}$$

Lemma 2.3. (see [10]) *Let $\varphi\in H^{r+3}(\Omega)$ and suppose that $\Phi:[0,T]\to\mathcal{R}(\mathcal{M}^0(\Delta))$ satisfies*

$$(\varphi_{xx}-\Phi_{xx})(\xi_{j,k})-(\varphi-\Phi)(\xi_{j,k})=0,\quad j=1,2,\cdots,N,\quad k=1,2. \tag{2.6}$$

Then we have

$$\|\varphi-\Phi\|_{L^2(\Omega)}\leq Ch^{r+1}\|\varphi\|_{H^{r+3}(\Omega)}. \tag{2.7}$$

2.2 Discretization of CNLS equations

We assume that the solutions of Eq. (1.1) have compact support on a bounded interval $[x_L,x_R]$ during the time interval $[0,T]$, i.e.,

$$\mathbf{i}\frac{\partial\varphi}{\partial t}+\frac{\partial^2\varphi}{\partial x^2}+(|\varphi|^2+\beta|\psi|^2)\varphi=0,\qquad x_L<x<x_R, \tag{2.8a}$$

$$\mathbf{i}\frac{\partial\psi}{\partial t}+\frac{\partial^2\psi}{\partial x^2}+(|\psi|^2+\beta|\varphi|^2)\psi=0,\qquad x_L<x<x_R, \tag{2.8b}$$

where φ and ψ are wave amplitudes in two polarizations and β is the cross-phase modulation coefficient, with initial conditions:

$$\varphi(x,0)=f(x), \qquad \psi(x,0)=g(x), \tag{2.9}$$

and boundary conditions:

$$\varphi(x_L,t)=\varphi(x_R,t)=0, \quad \psi(x_L,t)=\psi(x_R,t)=0, \quad t>0. \tag{2.10}$$

Two other different boundary conditions: the homogeneous Neumann boundary conditions:

$$\frac{\partial\varphi(x,t)}{\partial x}=\frac{\partial\psi(x,t)}{\partial x}=0, \qquad x=x_L, \qquad x=x_R, \tag{2.11}$$

and the periodic boundary conditions:

$$\varphi(x_L,t)=\varphi(x_R,t), \qquad \psi(x_L,t)=\psi(x_R,t), \qquad t>0. \tag{2.12}$$

In this paper, we mainly consider the boundary conditions Eq. (2.10), the boundary conditions Eqs. (2.11) and (2.12) can be used in the similar way. In Section 5, we give an example to present the efficiency and stability of our method to solve the periodic boundary conditions.

We propose the following continuous-time OSC scheme for Eqs. (2.8):

$$\begin{aligned}
&\left\{\mathbf{i}(\varphi_h^n)_t+(\varphi_h^{n+\frac{1}{2}})_{xx}+\left(|\varphi_h|^2+\beta|\psi_h|^2\right)^{n+\frac{1}{2}}\varphi_h^{n+\frac{1}{2}}\right\}(\xi_{j,k})=0,\\
&\left\{\mathbf{i}(\psi_h^n)_t+(\psi_h^{n+\frac{1}{2}})_{xx}+\left(|\psi_h|^2+\beta|\varphi_h|^2\right)^{n+\frac{1}{2}}\psi_h^{n+\frac{1}{2}}\right\}(\xi_{j,k})=0,
\end{aligned}$$

for $j=1,2,\cdots,N$; $n=0,1,2,\cdots,J-1$ and $k=1,2$. The corresponding discrete-time scheme is as follows:

$$\begin{aligned}
&\left\{\mathbf{i}\frac{\varphi_h^{n+1}-\varphi_h^n}{\tau}+\frac{(\varphi_h^{n+1})_{xx}+(\varphi_h^n)_{xx}}{2}\right.\\
&\qquad\left.+\frac{|\varphi_h^{n+1}|^2+|\varphi_h^n|^2+\beta\left(|\psi_h^{n+1}|^2+|\psi_h^n|^2\right)}{2}\frac{\varphi_h^{n+1}+\varphi_h^n}{2}\right\}(\xi_{j,k})=0, \qquad (2.13a)\\
&\left\{\mathbf{i}\frac{\psi_h^{n+1}-\psi_h^n}{\tau}+\frac{(\psi_h^{n+1})_{xx}+(\psi_h^n)_{xx}}{2}\right.\\
&\qquad\left.+\frac{|\psi_h^{n+1}|^2+|\psi_h^n|^2+\beta\left(|\varphi_h^{n+1}|^2+|\varphi_h^n|^2\right)}{2}\frac{\psi_h^{n+1}+\psi_h^n}{2}\right\}(\xi_{j,k})=0, \qquad (2.13b)
\end{aligned}$$

for $j=1,2,\cdots,N$; $n=0,1,2,\cdots,J-1$ and $k=1,2$.

3 Conservation laws

In this section, we study the conservation properties of the CNLS equations.

The solutions of Eq. (1.1) satisfy the following three conservation laws.

- **Mass conservation**:

$$I_1=\int_{-\infty}^{+\infty}|\varphi|^2dx=\text{const},\qquad I_2=\int_{-\infty}^{+\infty}|\psi|^2dx=\text{const};$$

- **Momentum conservation**:

$$I_3=\int_{-\infty}^{+\infty}\mathbf{i}\Big(\varphi\frac{\partial\bar{\varphi}}{\partial x}-\bar{\varphi}\frac{\partial\varphi}{\partial x}+\psi\frac{\partial\bar{\psi}}{\partial x}-\bar{\psi}\frac{\partial\psi}{\partial x}\Big)dx=\text{const};$$

- **Energy conservation**:

$$E=\int_{-\infty}^{+\infty}\Big(\Big|\frac{\partial\varphi}{\partial x}\Big|^2+\Big|\frac{\partial\psi}{\partial x}\Big|^2-\frac{1}{2}|\varphi|^4-\frac{1}{2}|\psi|^4-\beta|\varphi|^2|\psi|^2\Big)dx=\text{const}.$$

The corresponding discrete conservation laws are as follows:

(i) **Mass conservation**:

$$\begin{aligned}&I_1^{n+1}=\|\varphi_h^{n+1}\|_{\mathcal{G}}^2=I_1^n=\cdots=I_1^0=\text{const},\\&I_2^{n+1}=\|\psi_h^{n+1}\|_{\mathcal{G}}^2=I_2^n=\cdots=I_2^0=\text{const};\end{aligned}$$

(ii) **Momentum conservation**:

$$\begin{aligned}I_3^{n+1}=&\mathbf{i}\big\langle\varphi_h^{n+1},(\bar{\varphi}_h^{n+1})_x\big\rangle_{\mathcal{G}}-\mathbf{i}\big\langle\bar{\varphi}_h^{n+1},(\varphi_h^{n+1})_x\big\rangle_{\mathcal{G}}+\mathbf{i}\big\langle\psi_h^{n+1},(\bar{\psi}_h^{n+1})_x\big\rangle_{\mathcal{G}}\\&-\mathbf{i}\big\langle\bar{\psi}_h^{n+1},(\psi_h^{n+1})_x\big\rangle_{\mathcal{G}}=I_3^n=\cdots=I_3^0=\text{const};\end{aligned}$$

(iii) **Energy conservation**:

$$\begin{aligned}E^{n+1}=&\big\langle(\varphi_{h,1}^{n+1})_{xx},\varphi_{h,1}^{n+1}\big\rangle_{\mathcal{G}}+\big\langle(\varphi_{h,2}^{n+1})_{xx},\varphi_{h,2}^{n+1}\big\rangle_{\mathcal{G}}+\big\langle(\psi_{h,1}^{n+1})_{xx},\psi_{h,1}^{n+1}\big\rangle_{\mathcal{G}}\\&+\big\langle(\psi_{h,2}^{n+1})_{xx},\psi_{h,2}^{n+1}\big\rangle_{\mathcal{G}}+\frac{1}{2}\sum_{j=1}^{N}h_j\sum_{k=1}^{2}\omega_k\big(|\varphi_h^{n+1}|^4+|\psi_h^{n+1}|^4\big)\big(\xi_{j,k}\big)\\&+\sum_{j=1}^{N}h_j\sum_{k=1}^{2}\omega_k\beta|\varphi_h^{n+1}|^2|\psi_h^{n+1}|^2\big(\xi_{j,k}\big)=E^n=\cdots=E^0=\text{const}.\end{aligned}$$

Here for definition of $\varphi_{h,1}^{n+1}$, $\varphi_{h,2}^{n+1}$, $\psi_{h,1}^{n+1}$ and $\psi_{h,2}^{n+1}$, we refer to Eq. (3.4) later.

We try to prove these conservation laws one by one as follows.

The proof of (i): Computing the inner product of Eq. (2.13a) with $(\varphi_h^{n+1}+\varphi_h^n)$ and taking the imaginary part; and computing the inner product Eq. (2.13b) with $(\psi_h^{n+1}+\psi_h^n)$ and taking the imaginary part, we obtain

$$\|\varphi_h^{n+1}\|_{\mathcal{G}}^2=\|\varphi_h^n\|_{\mathcal{G}}^2,\qquad \|\psi_h^{n+1}\|_{\mathcal{G}}^2=\|\psi_h^n\|_{\mathcal{G}}^2.$$

Hence the mass conservation law is obtained.

The proof of (ii): For solitary waves collide, global momentum property is conserved. Computing the inner product of Eq. (2.13a) with $(\bar{\varphi}_h^{n+1})_x+(\bar{\varphi}_h^n)_x$ and subtracting the inner product of its complex conjugate with $(\varphi_h^{n+1})_x+(\varphi_h^n)_x$, we obtain

$$\begin{aligned}
&\mathbf{i}\Big\langle\frac{\varphi_h^{n+1}-\varphi_h^n}{\tau},(\bar{\varphi}_h^{n+1})_x+(\bar{\varphi}_h^n)_x\Big\rangle_{\mathcal{G}}+\frac{1}{2}\big\langle(\varphi_h^{n+1})_{xx}+(\varphi_h^n)_{xx},(\bar{\varphi}_h^{n+1})_x+(\bar{\varphi}_h^n)_x\big\rangle_{\mathcal{G}}\\
&\quad+\frac{1}{4}\big\langle\big(|\varphi_h^{n+1}|^2+|\varphi_h^n|^2+\beta(|\psi_h^{n+1}|^2+|\psi_h^n|^2)\big)(\varphi_h^{n+1}+\varphi_h^n),(\bar{\varphi}_h^{n+1}+\bar{\varphi}_h^n)_x\big\rangle_{\mathcal{G}}\\
&\quad-\mathbf{i}\Big\langle\frac{\bar{\varphi}_h^{n+1}-\bar{\varphi}_h^n}{\tau},(\varphi_h^{n+1})_x+(\varphi_h^n)_x\Big\rangle_{\mathcal{G}}-\frac{1}{2}\big\langle(\bar{\varphi}_h^{n+1})_{xx}+(\bar{\varphi}_h^n)_{xx},(\varphi_h^{n+1})_x+(\varphi_h^n)_x\big\rangle_{\mathcal{G}}\\
&\quad-\frac{1}{4}\big\langle\big(|\varphi_h^{n+1}|^2+|\varphi_h^n|^2+\beta(|\psi_h^{n+1}|^2+|\psi_h^n|^2)\big)(\bar{\varphi}_h^{n+1}+\bar{\varphi}_h^n),(\varphi_h^{n+1}+\varphi_h^n)_x\big\rangle_{\mathcal{G}}=0.
\end{aligned}\tag{3.1}$$

Note that for arbitrary complex functions φ and ψ, $\bar{\varphi}\psi-\varphi\bar{\psi}$ is an imaginary function. So taking the imaginary part of Eq. (3.1) gives

$$\begin{aligned}
&\mathbf{i}\Big\langle\frac{\varphi_h^{n+1}-\varphi_h^n}{\tau},(\bar{\varphi}_h^{n+1})_x+(\bar{\varphi}_h^n)_x\Big\rangle_{\mathcal{G}}-\mathbf{i}\Big\langle\frac{\bar{\varphi}_h^{n+1}-\bar{\varphi}_h^n}{\tau},(\varphi_h^{n+1})_x+(\varphi_h^n)_x\Big\rangle_{\mathcal{G}}\\
=&\frac{\mathbf{i}}{\tau}\big(\langle\varphi_h^{n+1},(\bar{\varphi}_h^{n+1})_x\rangle_{\mathcal{G}}-\langle\bar{\varphi}_h^{n+1},(\varphi_h^{n+1})_x\rangle_{\mathcal{G}}-\langle\varphi_h^n,(\bar{\varphi}_h^n)_x\rangle_{\mathcal{G}}+\langle\bar{\varphi}_h^n,(\varphi_h^n)_x\rangle_{\mathcal{G}}\big)\\
&+\frac{\mathbf{i}}{\tau}\big(\langle\varphi_h^{n+1},(\bar{\varphi}_h^n)_x\rangle_{\mathcal{G}}+\langle\bar{\varphi}_h^n,(\varphi_h^{n+1})_x\rangle_{\mathcal{G}}-\langle\varphi_h^n,(\bar{\varphi}_h^{n+1})_x\rangle_{\mathcal{G}}-\langle\bar{\varphi}_h^{n+1},(\varphi_h^n)_x\rangle_{\mathcal{G}}\big)\\
=&0.
\end{aligned}\tag{3.2}$$

Using Lemma 2.1, we observe that the second term of the middle side of (3.2) is zero. Consequently,

$$\begin{aligned}
I_{31}^{n+1}=&\mathbf{i}\langle\varphi_h^{n+1},(\bar{\varphi}_h^{n+1})_x\rangle_{\mathcal{G}}-\mathbf{i}\langle\bar{\varphi}_h^{n+1},(\varphi_h^{n+1})_x\rangle_{\mathcal{G}}=\mathbf{i}\langle\varphi_h^n,(\bar{\varphi}_h^n)_x\rangle_{\mathcal{G}}-\mathbf{i}\langle\bar{\varphi}_h^n,(\varphi_h^n)_x\rangle_{\mathcal{G}}\\
=&I_{31}^n=\cdots=I_{31}^0=\text{const.}
\end{aligned}$$

Similarly,

$$\begin{aligned}
I_{32}^{n+1}=&\mathbf{i}\langle\psi_h^{n+1},(\bar{\psi}_h^{n+1})_x\rangle_{\mathcal{G}}-\mathbf{i}\langle\bar{\psi}_h^{n+1},(\psi_h^{n+1})_x\rangle_{\mathcal{G}}=\mathbf{i}\langle\psi_h^n,(\bar{\psi}_h^n)_x\rangle_{\mathcal{G}}-\mathbf{i}\langle\bar{\psi}_h^n,(\psi_h^n)_x\rangle_{\mathcal{G}}\\
=&I_{32}^n=\cdots=I_{32}^0=\text{const.}
\end{aligned}$$

Therefore, we have

$$I_3^{n+1}=I_{31}^{n+1}+I_{32}^{n+1}=I_3^n=\cdots=I_3^0=\text{const.}$$

The momentum conservation law is obtained.

The proof of (iii): We compute the inner product of Eq. (2.13a) with $(\varphi_h^{n+1}-\varphi_h^n)$ and take the real part; and compute the inner product of Eq. (2.13b) with $(\psi_h^{n+1}-\psi_h^n)$ and take the real part and then obtain

$$E_1+E_2+E_3+E_4=0, \tag{3.3}$$

where

$$\begin{aligned}
E_1&=\mathrm{Re}\big(\langle(\varphi_h^{n+1})_{xx}+(\varphi_h^n)_{xx},\varphi_h^{n+1}-\varphi_h^n\rangle_{\mathcal{G}}\big),\\
E_2&=\frac{1}{2}\mathrm{Re}\big(\langle|\varphi_h^{n+1}|^2+|\varphi_h^n|^2+\beta(|\psi_h^{n+1}|^2+|\psi_h^n|^2)(\varphi_h^{n+1}+\varphi_h^n),\varphi_h^{n+1}-\varphi_h^n\rangle_{\mathcal{G}}\big),\\
E_3&=\mathrm{Re}\big(\langle(\psi_h^{n+1})_{xx}+(\psi_h^n)_{xx},\psi_h^{n+1}-\psi_h^n\rangle_{\mathcal{G}}\big),\\
E_4&=\frac{1}{2}\mathrm{Re}\big(\langle|\psi_h^{n+1}|^2+|\psi_h^n|^2+\beta(|\varphi_h^{n+1}|^2+|\varphi_h^n|^2)(\psi_h^{n+1}+\psi_h^n),\psi_h^{n+1}-\psi_h^n\rangle_{\mathcal{G}}\big).
\end{aligned}$$

Here $\mathrm{Re}(\cdot)$ denotes taking the real part of the argument. Setting

$$\varphi_h^n=\varphi_{h,1}^n+\mathbf{i}\varphi_{h,2}^n,\qquad \psi_h^n=\psi_{h,1}^n+\mathbf{i}\psi_{h,2}^n, \tag{3.4}$$

where $\varphi_{h,1}^n$ and $\varphi_{h,2}^n$ are real and imaginary parts of φ_h^n, $\psi_{h,1}^n$ and $\psi_{h,2}^n$ are real and imaginary parts of ψ_h^n, we obtain

$$\begin{aligned}
E_1=&\mathrm{Re}\big(\langle(\varphi_h^{n+1})_{xx}+(\varphi_h^n)_{xx},\varphi_h^{n+1}-\varphi_h^n\rangle_{\mathcal{G}}\big)\\
=&\sum_{j=1}^{N}h_j\sum_{k=1}^{2}\omega_k\big(\langle(\varphi_{h,1}^{n+1})_{xx},\varphi_{h,1}^{n+1}-\varphi_{h,1}^n\rangle_{\mathcal{G}}+\langle(\varphi_{h,2}^{n+1})_{xx},\varphi_{h,2}^{n+1}-\varphi_{h,2}^n\rangle_{\mathcal{G}}\big)(\xi_{j,k})\\
&+\sum_{j=1}^{N}h_j\sum_{k=1}^{2}\omega_k\big(\langle(\varphi_{h,1}^n)_{xx},\varphi_{h,1}^{n+1}-\varphi_{h,1}^n\rangle_{\mathcal{G}}+\langle(\varphi_{h,2}^n)_{xx},\varphi_{h,2}^{n+1}-\varphi_{h,2}^n\rangle_{\mathcal{G}}\big)(\xi_{j,k})\\
=&\big(\langle(\varphi_{h,1}^{n+1})_{xx},\varphi_{h,1}^{n+1}\rangle_{\mathcal{G}}+\langle(\varphi_{h,2}^{n+1})_{xx},\varphi_{h,2}^{n+1}\rangle_{\mathcal{G}}-\langle(\varphi_{h,1}^{n+1})_{xx},\varphi_{h,1}^n\rangle_{\mathcal{G}}-\langle(\varphi_{h,2}^{n+1})_{xx},\varphi_{h,2}^n\rangle_{\mathcal{G}}\big)\\
&+\big(\langle(\varphi_{h,1}^{n+1})_{xx},\varphi_{h,1}^n\rangle_{\mathcal{G}}+\langle(\varphi_{h,2}^{n+1})_{xx},\varphi_{h,2}^n\rangle_{\mathcal{G}}-\langle(\varphi_{h,1}^n)_{xx},\varphi_{h,1}^n\rangle_{\mathcal{G}}-\langle(\varphi_{h,2}^n)_{xx},\varphi_{h,2}^n\rangle_{\mathcal{G}}\big)\\
=&\langle(\varphi_{h,1}^{n+1})_{xx},\varphi_{h,1}^{n+1}\rangle_{\mathcal{G}}+\langle(\varphi_{h,2}^{n+1})_{xx},\varphi_{h,2}^{n+1}\rangle_{\mathcal{G}}-\langle(\varphi_{h,1}^n)_{xx},\varphi_{h,1}^n\rangle_{\mathcal{G}}-\langle(\varphi_{h,2}^n)_{xx},\varphi_{h,2}^n\rangle_{\mathcal{G}}.
\end{aligned}\tag{3.5}$$

By using Lemma 2.1, we get

$$\begin{aligned}
E_2=&\frac{1}{2}\mathrm{Re}\big(\langle\big(|\varphi_h^{n+1}|^2+|\varphi_h^n|^2+\beta(|\psi_h^{n+1}|^2+|\psi_h^n|^2)\big)(\varphi_h^{n+1}+\varphi_h^n),\varphi_h^{n+1}-\varphi_h^n\rangle_{\mathcal{G}}\big)\\
=&\frac{1}{2}\sum_{j=1}^{N}h_j\sum_{k=1}^{2}\omega_k\big(|\varphi_h^{n+1}|^2+|\varphi_h^n|^2+\beta(|\psi_h^{n+1}|^2+|\psi_h^n|^2)\big)\big(|\varphi_h^{n+1}|^2-|\varphi_h^n|^2\big)(\xi_{j,k})\\
=&\frac{1}{2}\sum_{j=1}^{N}h_j\sum_{k=1}^{2}\omega_k\big(|\varphi_h^{n+1}|^4-|\varphi_h^n|^4+\beta(|\psi_h^{n+1}|^2+|\psi_h^n|^2)\big(|\varphi_h^{n+1}|^2-|\varphi_h^n|^2\big)\big)(\xi_{j,k}).
\end{aligned}\tag{3.6}$$

Similarly,

$$E_3=\left\langle(\psi_{h,1}^{n+1})_{xx},\psi_{h,1}^{n+1}\right\rangle_{\mathcal{G}}+\left\langle(\psi_{h,2}^{n+1})_{xx},\psi_{h,2}^{n+1}\right\rangle_{\mathcal{G}}-\left\langle(\psi_{h,1}^{n})_{xx},\psi_{h,1}^{n}\right\rangle_{\mathcal{G}}-\left\langle(\psi_{h,2}^{n})_{xx},\psi_{h,2}^{n}\right\rangle_{\mathcal{G}}, \tag{3.7}$$

$$E_4=\frac{1}{2}\sum_{j=1}^{N}h_j\sum_{k=1}^{2}\omega_k\big(|\psi_h^{n+1}|^4-|\psi_h^n|^4+\beta(|\varphi_h^{n+1}|^2+|\varphi_h^n|^2)\big(|\psi_h^{n+1}|^2-|\psi_h^n|^2\big)\big)(\xi_{j,k}). \tag{3.8}$$

Substituting (3.5)-(3.8) into (3.3), we obtain

$$\begin{aligned}E^{n+1}\triangleq&\left\langle(\varphi_{h,1}^{n+1})_{xx},\varphi_{h,1}^{n+1}\right\rangle_{\mathcal{G}}+\left\langle(\varphi_{h,2}^{n+1})_{xx},\varphi_{h,2}^{n+1}\right\rangle_{\mathcal{G}}+\left\langle(\psi_{h,1}^{n+1})_{xx},\psi_{h,1}^{n+1}\right\rangle_{\mathcal{G}}+\left\langle(\psi_{h,2}^{n+1})_{xx},\psi_{h,2}^{n+1}\right\rangle_{\mathcal{G}}\\&+\frac{1}{2}\sum_{j=1}^{N}h_j\sum_{k=1}^{2}\omega_k\big(|\varphi_h^{n+1}|^4+|\psi_h^{n+1}|^4\big)(\xi_{j,k})+\sum_{j=1}^{N}h_j\sum_{k=1}^{2}\omega_k\beta|\varphi_h^{n+1}|^2|\psi_h^{n+1}|^2(\xi_{j,k})\\=&\left\langle(\varphi_{h,1}^{n})_{xx},\varphi_{h,1}^{n}\right\rangle_{\mathcal{G}}+\left\langle(\varphi_{h,2}^{n})_{xx},\varphi_{h,2}^{n}\right\rangle_{\mathcal{G}}+\left\langle(\psi_{h,1}^{n})_{xx},\psi_{h,1}^{n}\right\rangle_{\mathcal{G}}+\left\langle(\psi_{h,2}^{n})_{xx},\psi_{h,2}^{n}\right\rangle_{\mathcal{G}}\\&+\frac{1}{2}\sum_{j=1}^{N}h_j\sum_{k=1}^{2}\omega_k\big(|\varphi_h^{n}|^4+|\psi_h^{n}|^4\big)(\xi_{j,k})+\sum_{j=1}^{N}h_j\sum_{k=1}^{2}\omega_k\beta|\varphi_h^{n}|^2|\psi_h^{n}|^2(\xi_{j,k})\\\triangleq&E^n.\end{aligned}$$

The energy conservation law is proved.

4 Accuracy and stability of the scheme

In this section, we study the accuracy and stability of the numerical method.

Theorem 4.1. *Suppose* $\varphi,\psi\in C^{2,4}\cap L^2(0,T;H^{r+3})$ *are the solution of* (2.8), $\partial\varphi/\partial t$, $\partial\psi/\partial t$, $\partial^2\varphi/\partial t^2$, $\partial\psi^2/\partial t^2\in L^2(0,T;H^{r+3})$, *while* $\varphi_h^n,\psi_h^n\in\mathcal{M}^0(\Delta)(n=0,1,\cdots,J-1)$ *are the solutions of* (2.13). *If* $\Phi,\Psi:[0,T]\to\mathcal{M}^0(\Delta)$ *are defined by* (2.6) *and* $\|\varphi_h^0-\Phi^0\|_{L^2(\Omega)}$, $\|\psi_h^0-\Psi^0\|_{L^2(\Omega)}$ *are* $\mathcal{O}(\tau^2+h^4)^2$, *then for* τ *and* h *sufficiently small, we have*

$$\|\varphi^J-\varphi_h^J\|_\infty+\|\psi^J-\psi_h^J\|_\infty=\mathcal{O}(\tau^2+h^4), \tag{4.1}$$

where $\varphi^n(x)=\varphi(x,n\tau)$, $\psi^n(x)=\psi(x,n\tau)$ *are the exact solution of* (2.8) *when* $t=n\tau$.

Proof. Substituting $\varphi^n(x),\psi^n(x)$ into (2.13) and using Taylor expansion at $t=n+\frac{1}{2}$, we have

$$R_1^n(\xi_{j,k})=\frac{\mathrm{i}}{\tau}(\varphi^{n+1}-\varphi^n)+(\varphi^{n+\frac{1}{2}})_{xx}+(|\varphi|^2+\beta|\psi|^2)^{n+\frac{1}{2}}\varphi^{n+\frac{1}{2}}=\mathcal{O}(\tau^2), \tag{4.2a}$$

$$R_2^n(\xi_{j,k})=\frac{\mathrm{i}}{\tau}(\psi^{n+1}-\psi^n)+(\psi^{n+\frac{1}{2}})_{xx}+(|\psi|^2+\beta|\varphi|^2)^{n+\frac{1}{2}}\psi^{n+\frac{1}{2}}=\mathcal{O}(\tau^2). \tag{4.2b}$$

Here R_1^n and R_2^n are truncation errors. Let

$$\hat{e}_1^n=\varphi^n-\Phi^n,\qquad e_1^n=\varphi_h^n-\Phi^n,\qquad \hat{e}_2^n=\psi^n-\Psi^n,\qquad e_2^n=\psi_h^n-\Psi^n.$$

Then we have

$$\varphi^n-\varphi_h^n=\hat{e}_1^n-e_1^n,\qquad \psi^n-\psi_h^n=\hat{e}_2^n-e_2^n.$$

For simplicity, we only give the process of Eq. (4.2a). Let

$$G(\varphi^n)=(|\varphi|^2+\beta|\psi|^2)^{n+\frac{1}{2}}.$$

Subtracting (2.13) from (4.2a), we have

$$\begin{aligned}&\frac{\mathrm{i}}{\tau}(e_1^{n+1}-e_1^n)+(e_1^{n+\frac{1}{2}})_{xx}\\ =&\frac{\mathrm{i}}{\tau}(\hat{e}_1^{n+1}-\hat{e}_1^n)+(\hat{e}_1^{n+\frac{1}{2}})_{xx}-R_1^n+\big(G(\varphi^n)-G(\varphi_h^n)\big)\varphi_n^{n+\frac{1}{2}}+G(\varphi^n)(\hat{e}_1^{n+\frac{1}{2}}-e_1^{n+\frac{1}{2}}).\end{aligned}\tag{4.3}$$

Computing the inner product of (4.3) with $e_1^{n+1}+e_1^n$ and taking the imaginary part, we obtain

$$\|e_1^{n+1}\|_{\mathcal{G}}^2-\|e_1^n\|_{\mathcal{G}}^2=\Pi_1+\Pi_2+\Pi_3,\tag{4.4}$$

where

$$\begin{aligned}\Pi_1=&\,\mathrm{Im}\langle\hat{e}_1^{n+1}-\hat{e}_1^n,e_1^{n+1}+e_1^n\rangle_{\mathcal{G}}+\tau\mathrm{Im}\langle(\hat{e}_1^{n+\frac{1}{2}})_{xx}-R_1^n,e_1^{n+1}+e_1^n\rangle_{\mathcal{G}}\\ =&\,\tau\mathrm{Im}\big\langle(\hat{e}_1^n)_t+(\hat{e}_1^{n+\frac{1}{2}})_{xx}-R_1^n,e_1^{n+1}+e_1^n\big\rangle_{\mathcal{G}}\\ \le&\,C\tau\big(\|(\hat{e}_1^n)_t\|_{\mathcal{G}}^2+\|(\hat{e}_1^{n+\frac{1}{2}})_{xx}\|_{\mathcal{G}}^2+\|R_1^n\|_{\mathcal{G}}^2+\|e_1^{n+\frac{1}{2}}\|_{\mathcal{G}}^2\big),\\ \Pi_2=&\,\tau\mathrm{Im}\big\langle\big(G(\varphi^n)-G(\varphi_h^n)\big)\varphi_h^{n+\frac{1}{2}},e_1^{n+1}+e_1^n\big\rangle_{\mathcal{G}},\\ \Pi_3=&\,\tau\mathrm{Im}\big\langle G(\varphi^n)(\hat{e}_1^{n+\frac{1}{2}}-e_1^{n+\frac{1}{2}}),e_1^{n+1}+e_1^n\big\rangle_{\mathcal{G}}\\ \le&\,C\tau\big(\|\hat{e}_1^{n+\frac{1}{2}}\|_{\mathcal{G}}^2+\|e_1^{n+\frac{1}{2}}\|_{\mathcal{G}}^2\big).\end{aligned}$$

Here $\mathrm{Im}(\cdot)$ denotes taking the imaginary part of the argument. For Π_2, we have by a direct calculation that

$$\begin{aligned}&G(\varphi^n)-G(\varphi_h^n)\\ =&\frac{1}{2}\Big(\varphi^{n+1}\bar{\varphi}^{n+1}-\varphi_h^{n+1}\bar{\varphi}_h^{n+1}+\varphi^n\bar{\varphi}^n-\varphi_h^n\bar{\varphi}_h^n\Big)+\frac{\beta}{2}\Big(\psi^{n+1}\bar{\psi}^{n+1}-\psi_h^{n+1}\bar{\psi}_h^{n+1}+\psi^n\bar{\psi}^n-\psi_h^n\bar{\psi}_h^n\Big)\\ =&\frac{1}{2}\Big(\varphi^{n+1}(\bar{\hat{e}}_1^{n+1}-\bar{e}_1^{n+1})+\bar{\varphi}_h^{n+1}(\hat{e}_1^{n+1}-e_1^{n+1})+\varphi^n(\bar{\hat{e}}_1^n-\bar{e}_1^n)+\bar{\varphi}_h^n(\hat{e}_1^n-e_1^n)\Big)\\ &+\frac{\beta}{2}\Big(\psi^{n+1}(\bar{\hat{e}}_2^{n+1}-\bar{e}_2^{n+1})+\bar{\psi}_h^{n+1}(\hat{e}_2^{n+1}-e_2^{n+1})+\psi^n(\bar{\hat{e}}_2^n-\bar{e}_2^n)+\bar{\psi}_h^n(\hat{e}_2^n-e_2^n)\Big).\end{aligned}$$

According to the assumptions of the theorem, φ^n, φ_h^n, ψ^n, ψ_h^n are bounded, therefore

$$\Pi_2\le C\tau\Big(\|\hat{e}_1^{n+1}\|_{\mathcal{G}}^2+\|e_1^{n+1}\|_{\mathcal{G}}^2+\|\hat{e}_1^n\|_{\mathcal{G}}^2+\|e_1^n\|_{\mathcal{G}}^2+\|\hat{e}_2^{n+1}\|_{\mathcal{G}}^2+\|e_2^{n+1}\|_{\mathcal{G}}^2+\|\hat{e}_2^n\|_{\mathcal{G}}^2+\|e_2^n\|_{\mathcal{G}}^2\Big).$$

From the above analysis, (4.4) implies

$$\begin{aligned}&\|e_1^{n+1}\|_{\mathcal{G}}^2-\|e_1^n\|_{\mathcal{G}}^2\\&\leq C\tau\Big(\|(\hat{e}_1^n)_t\|_{\mathcal{G}}^2+\|(\hat{e}_1^{n+\frac{1}{2}})_{xx}\|_{\mathcal{G}}^2+\|R_1^n\|_{\mathcal{G}}^2+\|e_1^{n+\frac{1}{2}}\|_{\mathcal{G}}^2+\|\hat{e}_1^{n+\frac{1}{2}}\|_{\mathcal{G}}^2+\|e_2^{n+\frac{1}{2}}\|_{\mathcal{G}}^2+\|\hat{e}_2^{n+\frac{1}{2}}\|_{\mathcal{G}}^2\Big).\end{aligned}$$

According to the definite of Φ^n, one can easily obtain $(\hat{e}_1^{n+1/2})_{xx}=\hat{e}_1^{n+1/2}$. From (4.2a), we obtain $R_1^n=\mathcal{O}(\tau^2)$. Those conditions together with Lemma 2.3 yield

$$\begin{aligned}\|(\hat{e}_1^n)_t\|_{\mathcal{G}}&=\Big\|\frac{\hat{e}_1^{n+1}-\hat{e}_1^n}{\tau}\Big\|_{\mathcal{G}}=\Big\|\frac{\varphi^{n+1}-\varphi^n-(\Phi^{n+1}-\Phi^n)}{\tau}\Big\|_{\mathcal{G}}\leq Ch^{r+1}\Big\|\frac{\varphi^{n+1}-\varphi^n}{\tau}\Big\|_{H^{r+3}}\\&=Ch^{r+1}\Big\|\frac{1}{\tau}\int_{n\tau}^{n\tau+\tau}\frac{\partial\varphi}{\partial t}dt\Big\|_{H^{r+3}}=Ch^{r+1}\Big\|\frac{1}{\tau}\int_0^{\tau}\frac{\partial\varphi(s+n\tau)}{\partial s}ds\Big\|_{H^{r+3}}\\&\leq Ch^{r+1}\frac{1}{\tau}\int_0^{\tau}\Big\|\frac{\partial\varphi(s+n\tau)}{\partial s}\Big\|_{H^{r+3}}ds\\&\leq Ch^{r+1}\Big(\Big\|\frac{\partial\varphi}{\partial t}\Big\|_{L^\infty(0,T;H^{r+3})}+\|\varphi\|_{L^\infty(0,T;H^{r+2})}\Big)\leq Ch^{r+1}.\end{aligned}$$

By using (2.1) and Lemma 2.1, one can get

$$\begin{aligned}&\|\hat{e}_1^n\|_{\mathcal{G}}^2\leq C\|\hat{e}_1^n\|_{L^2}^2\leq Ch^{r+1}\|\varphi^n\|_{H^{r+3}}\leq C(h^{r+1})^2,\\&\|\hat{e}_2^n\|_{\mathcal{G}}^2\leq C\|\hat{e}_2^n\|_{L^2}^2\leq Ch^{r+1}\|\psi^n\|_{H^{r+3}}\leq C(h^{r+1})^2.\end{aligned}$$

Thus (4.4) can be written in the following form

$$\|e_1^{n+1}\|_{\mathcal{G}}^2-\|e_1^n\|_{\mathcal{G}}^2\leq C\tau\Big(\|e_1^{n+\frac{1}{2}}\|_{\mathcal{G}}^2+\|e_2^{n+\frac{1}{2}}\|_{\mathcal{G}}^2\Big)+C\tau\big(\tau^2+h^{r+1}\big)^2. \tag{4.5}$$

Similarly, we obtain

$$\|e_2^{n+1}\|_{\mathcal{G}}^2-\|e_2^n\|_{\mathcal{G}}^2\leq C\tau\Big(\|e_1^{n+\frac{1}{2}}\|_{\mathcal{G}}^2+\|e_2^{n+\frac{1}{2}}\|_{\mathcal{G}}^2\Big)+C\tau\big(\tau^2+h^{r+1}\big)^2. \tag{4.6}$$

In the following, C_i, $i=1,\cdots,10$, denote generic constants. Summing up both sides of Eq. (4.5) and Eq. (4.6) from 0 to $J-1$, we have

$$\begin{aligned}\|e_1^J\|_{\mathcal{G}}^2\leq{}&C_1\tau\|e_1^J\|_{\mathcal{G}}^2+(1+C_1\tau)\|e_1^0\|_{\mathcal{G}}^2+C_1\tau\|e_2^0\|_{\mathcal{G}}^2\\&+C_2\tau\sum_{n=1}^{J-1}\Big(\|e_1^n\|_{\mathcal{G}}^2+\|e_2^n\|_{\mathcal{G}}^2\Big)+C_3\tau\sum_{n=0}^{J-1}\big(\tau^2+h^{r+1}\big)^2,\end{aligned} \tag{4.7a}$$

$$\begin{aligned}\|e_2^J\|_{\mathcal{G}}^2\leq{}&C_4\tau\|e_2^J\|_{\mathcal{G}}^2+(1+C_4\tau)\|e_2^0\|_{\mathcal{G}}^2+C_4\tau\|e_1^0\|_{\mathcal{G}}^2\\&+C_5\tau\sum_{n=1}^{J-1}\Big(\|e_2^n\|_{\mathcal{G}}^2+\|e_1^n\|_{\mathcal{G}}^2\Big)+C_6\tau\sum_{n=0}^{J-1}\big(\tau^2+h^{r+1}\big)^2.\end{aligned} \tag{4.7b}$$

Combining Eq. (4.7a) with Eq. (4.7b), we obtain

$$\begin{aligned}&(1-C_7\tau)\left(\|e_1^J\|_{\mathcal{G}}^2+\|e_2^J\|_{\mathcal{G}}^2\right)\\ \leq&(1+C_8\tau)\left(\|e_1^0\|_{\mathcal{G}}^2+\|e_2^0\|_{\mathcal{G}}^2\right)+C_9\tau\sum_{n=1}^{J-1}\left(\tau^2+h^{r+1}\right)^2+C_{10}\tau\sum_{n=1}^{J-1}\left(\|e_1^n\|_{\mathcal{G}}+\|e_2^n\|_{\mathcal{G}}\right).\end{aligned}$$

Let τ be small enough so that $1-C_1\tau>0$. We get by use of the Gronwall inequality,

$$\begin{aligned}\|e_1^J\|_{\mathcal{G}}^2+\|e_2^J\|_{\mathcal{G}}^2\leq&\left((1+C\tau)\left(\|e_1^0\|_{\mathcal{G}}^2+\|e_2^0\|_{\mathcal{G}}^2\right)+C\tau\sum_{n=0}^{J-1}(\tau^2+h^{r+1})^2\right)\exp(CJ\tau)\\ \leq&\|e_1^0\|_{\mathcal{G}}^2+\|e_2^0\|_{\mathcal{G}}^2+(\tau^2+h^{r+1})^2.\end{aligned}$$

From the assumptions of the theorem, we obtain

$$\|e_1^J\|_{\mathcal{G}}^2+\|e_2^J\|_{\mathcal{G}}^2\leq C(\tau^2+h^{r+1})^2.$$

By using (2.1), we have

$$\|e_1^J\|_{L^2}^2+\|e_2^J\|_{L^2}^2\leq C(\tau^2+h^{r+1})^2.$$

Finally, by using the concept of equivalent norms,

$$\|e_1^J\|_\infty+\|e_2^J\|_\infty\leq C(\tau^2+h^{r+1})^2=C(\tau^2+h^4)^2.$$

So, the proof is complete. □

In the following theorem, we give the stability of the numerical method.

Theorem 4.2. *If the conditions of Theorem* 4.1 *are satisfied, then the scheme* (2.13) *depends on the initial value continuously.*

Proof. By a similar proof as that of Theorem 4.1, one can easily obtain

$$\|e_1^J\|_\infty^2+\|e_2^J\|_\infty^2\leq C\left(\|e_1^0\|^2+\|e_2^0\|^2\right),$$

which implies that (2.13) depends on the initial value continuously. □

5 Numerical results

In this section, we provide numerical examples to illustrate the accuracy and capability of methods developed in previous sections.

Since (2.13) is a nonlinear scheme, one should utilize some iterative method to solve it. One possible choice is given below:

$$\left\{\mathbf{i}\frac{(\varphi_h^{n+1})^{(s+1)}-\varphi_h^n}{\tau}+\frac{(\varphi_h^{n+1})_{xx}^{(s+1)}+(\varphi_h^n)_{xx}}{2}\right.$$
$$\left.+\frac{|(\varphi_h^{n+1})^{(s)}|^2+|\varphi_h^n|^2+\beta\big(|(\psi_h^{n+1})^{(s)}|^2+|\psi_h^n|^2\big)}{2}\frac{(\varphi_h^{n+1})^{(s+1)}+\varphi_h^n}{2}\right\}(\xi_{j,k})=0, \quad (5.1a)$$

$$\left\{\mathbf{i}\frac{(\psi_h^{n+1})^{(s+1)}-\psi_h^n}{\tau}+\frac{(\psi_h^{n+1})_{xx}^{(s+1)}+(\psi_h^n)_{xx}}{2}\right.$$
$$\left.+\frac{|(\psi_h^{n+1})^{(s)}|^2+|\psi_h^n|^2+\beta\big(|(\varphi_h^{n+1})^{(s)}|^2+|\varphi_h^n|^2\big)}{2}\frac{(\psi_h^{n+1})^{(s+1)}+\psi_h^n}{2}\right\}(\xi_{j,k})=0, \quad (5.1b)$$

for $j=1,2,\cdots,N$; $n=0,1,2,\cdots,J-1$ and $k=1,2$, where s denotes the s-th iteration at a given time-step and the iteration continues until the condition

$$\max_{\substack{1\le j\le N\\ k=1,2}}|(\varphi_h^{n+1})^{(s+1)}(\xi_{j,k})-(\varphi_h^{n+1})^{(s)}(\xi_{j,k})|+\max_{\substack{1\le j\le N\\ k=1,2}}|(\psi_h^{n+1})^{(s+1)}(\xi_{j,k})-(\psi_h^{n+1})^{(s)}(\xi_{j,k})|<10^{-6}$$

is reached. Setting

$$\vec{\varphi}^n=[\hat{\varphi}_1^n,\hat{\varphi}_2^n,\cdots,\hat{\varphi}_{2N}^n]^T, \qquad \vec{\psi}^n=[\hat{\psi}_1^n,\hat{\psi}_2^n,\cdots,\hat{\psi}_{2N}^n]^T$$

and substituting (2.2) into (5.1), one can obtain

$$A(\vec{\varphi}^{n+1})^{(s+1)}=(\vec{c}_h^{n+1})^{(s)}, \qquad B(\vec{\psi}^{n+1})^{(s+1)}=(\vec{d}_h^{n+1})^{(s)},$$

where $(\vec{c}_h^{n+1})^{(s)}$ is a vector which composes of $(\varphi_h^{n+1})^{(s)}$, $(\psi_h^{n+1})^{(s)}$, $(\varphi_h^n)_{xx}$, φ_h^n, ψ_h^n and $(\vec{d}_h^{n+1})^{(s)}$ is a vector which composes of $(\varphi_h^{n+1})^{(s)}$, $(\psi_h^{n+1})^{(s)}$, $(\psi_h^n)_{xx}$, ψ_h^n, φ_h^n, both A and B are matrix with special structure.

Now we consider (1.1) with the following soliton solution [24]:

$$\varphi(x,t)=\sqrt{\frac{2\alpha_1}{1+\beta}}\mathrm{sech}\big(\sqrt{\alpha}_1(x-2v_1t)\big)\exp\big(\mathbf{i}(v_1x-(v_1^2-\alpha_1)t)\big), \quad (5.2a)$$

$$\psi(x,t)=\sqrt{\frac{2\alpha_2}{1+\beta}}\mathrm{sech}\big(\sqrt{\alpha}_2(x-2v_2t)\big)\exp\big(\mathbf{i}(v_2x-(v_2^2-\alpha_2)t)\big), \quad (5.2b)$$

where α_i and v_i $(i=1,2)$ are arbitrary constants.

We test conserved quantities and the order of convergence. In addition, we make some comparisons with other schemes and it proves that the scheme in the paper does have high accuracy and efficiency. We study single solitary wave propagation, double solitary wave propagation, various kinds of collisions of two different vector solitons and periodic boundary conditions. We consider the following problems to highlight the properties of the derived scheme.

5.1 Single soliton

In this test we choose the initial condition from the soliton solution (5.2)

$$\varphi(x,0)=\psi(x,0)=\sqrt{\frac{2\alpha}{1+\beta}}\operatorname{sech}(\sqrt{\alpha}x)\exp(\mathbf{i}vx),$$

where α, β and v are constants.

To compute the numerical solution, the following parameters are used

$$x_L=-30,\quad x_R=60,\quad v=0.5,\quad \alpha=0.2,\quad \beta=1,\quad h=0.1,\quad \tau=0.01,\quad T=24.$$

Perspective views of the traveling soliton are presented in Fig. 1. To demonstrate the high accuracy of the OSC method, we use the same procedure as that in [19] which emphasizes that a good numerical scheme should have excellent long-time numerical behavior, as well as conservation properties. In Table 1, we display the conserved quantities obtained from the proposed scheme. It is very easy to see that all of them are exactly conserved. It shows that the proposed method is stable and preserves conserved properties well. The number of iterations shows the efficiency of the method.

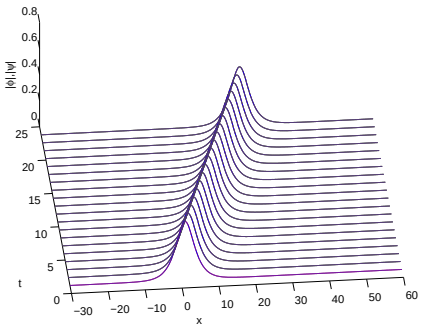

Figure 1: Single soliton at difference time levels.

The rate of convergence of the proposed method can be calculated from the formula [13]

$$p=\log\Big(\frac{\|\varphi-\varphi_{h_1}\|_\infty}{\|\varphi-\varphi_{h_2}\|_\infty}\Big)\Big/\log\Big(\frac{h_1}{h_2}\Big),$$

where h_1, h_2 are space steps and the value of p is called the rate of convergence. In Theorem 4.1, we prove that our proposed scheme is fourth-order in space and second-order in time. For this computation we choose the time step $\tau=h^2$ as we expect the scheme to be second order accurate in time and fourth order accurate in space in the discrete maximum norm and L^2 norm respectively. Table 2 confirms our conclusion. We can see that the numbers in the last column in Table 2 are more than four, which shows fourth order accurate in space. As we choose the time step $\tau=h^2$, the scheme is second order accurate in time. The results are obtained in the final time $T=24$.

Table 1: Conserved quantities (single soliton).

Time	I_1	I_3	E	Iter. No.
0.0	1.78885431	-3.57770839	-0.65591323	3
6.0	1.78885431	-3.57770839	-0.65591323	3
12.0	1.78885431	-3.57770839	-0.65591323	3
18.0	1.78885431	-3.57770839	-0.65591323	3
24.0	1.78885431	-3.57770839	-0.65591323	3

Table 2: Rate of convergence.

h	τ	$\|\varphi-\Phi\|_\infty$	order
1.0	1.0	0.04708139	-
0.5	0.25	0.00276749	4.0885
0.25	0.0625	1.72790606e-04	4.0015
0.125	0.015625	1.07464795e-05	4.0071

In Fig. 2, a comparison of the OSC scheme with the CN scheme [14], the Ismail scheme [13] and the Wang scheme [23] has been made. Though our scheme and the Ismail scheme have the same fourth-order in space and second-order in time, our algorithm is easy to implement. In fact, our scheme is more accurate than the Ismail scheme.

5.2 Two solitons with same initial values

Let us consider the interaction of two solitons as examples to test the stability. We use the initial condition

$$\varphi(x,0)=\psi(x,0)=\sum_{j=1,2}\sqrt{\frac{2\alpha_j}{1+\beta}}\mathrm{sech}(\sqrt{\alpha}_j x-x_j)\exp\{\mathbf{i}v_j x\}.$$

In our numerical calculations we choose parameters

$$\begin{array}{lllll} x_L=0, & x_R=60, & \alpha_1=\alpha_2=1, & \beta=1, & \\ x_1=20, & x_2=45, & v_1=0.5, & v_2=-0.5, & T=30. \end{array}$$

Table 3: Two solitons with same initial values (conserved quantities).

Time	I_1	I_3	E	Iter. No.
0.0	7.99753656	-0.01773143	-2.22130218	4
6.0	7.99753656	-0.01620189	-2.22130214	3
12.0	7.99753656	-0.01546758	-2.22130212	4
18.0	7.99753656	-0.01560848	-2.22130211	3
24.0	7.99753656	-0.01692837	-2.22130205	3
30.0	7.99753656	-0.01576484	-2.22130202	3

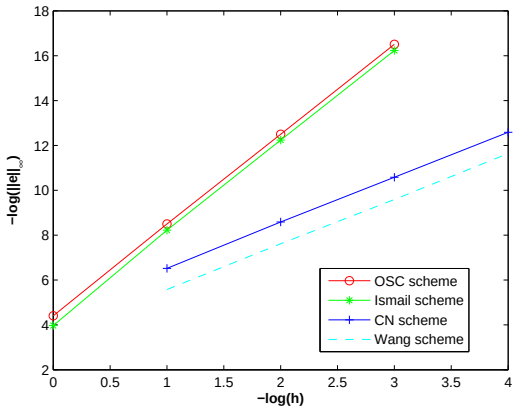

Figure 2: Convergence rate of four different schemes.

When $\beta=1$, the equations are integrable, solitary waves collide elastically. As wave velocity has the same absolute value and $\alpha_1=\alpha_2$ keeps the same, so two waves transmit without any change to the same direction at the same rate. Fig. 3(a) gives the perspective views of the traveling two solitons at difference time with the same initial values. We can see that after the collision of two solitons, they move in the same direction and with the same velocity as before. Fig. 3(b) shows contours of the interaction scenario. We observe that sympathia phenomenon takes place at $t=12$. Table 3 shows that I_3 varies from time to time as collision happens, but the global momentums keep the same. High mass and energy conservation quantities have been conserved during the interaction scenario.

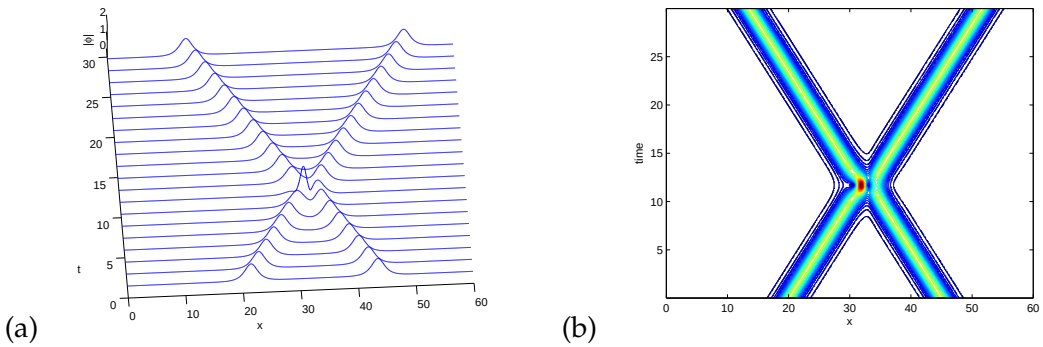

(a) (b)

Figure 3: (a) Waves of two solitons; (b) contours of two solitons.

5.3 Soliton collisions of different initial conditions

In this section, we solve (2.8) together with different initial condition. In the following calculations, we fix $x_L=-40$, $x_R=40$,

Table 4: Two solitons interaction $\beta=1$ (conserved quantities).

Time	I_1	I_2	I_3	E	Iter. No.
0.0	9.59990132	7.99995731	-0.79981944	6.17443445	6
20.0	9.59990132	7.99995731	-0.79975390	6.17443473	6
40.0	9.59990132	7.99995731	-0.79980237	6.17443502	6
60.0	9.59990132	7.99995731	-0.79980010	6.17443530	6
80.0	9.59990132	7.99995731	-0.79979386	6.17443558	6

Table 5: Conserved quantities ($\beta=0.3$, $v=0.4$).

Time	I_1	I_2	I_3	E	Iter. No.
0.0	9.59999779	7.99999909	-0.31999819	7.09866028	5
20.0	9.59999779	7.99996509	-0.31999775	7.09866033	5
40.0	9.59999779	7.99996509	-0.32007717	7.09866040	5
60.0	9.59999779	7.99996509	-0.23995993	7.09866049	5
80.0	9.59999779	7.99996509	-0.52739889	7.09866054	5

$$\varphi(x,0)=\sqrt{2\alpha_1}\mathrm{sech}(\sqrt{2\alpha_1}x+x_{1,0})\exp(\mathbf{i}v_1x),$$
$$\psi(x,0)=\sqrt{2\alpha_2}\mathrm{sech}(\sqrt{2\alpha_2}x+x_{2,0})\exp(\mathbf{i}v_2x),$$

where amplitudes are $\sqrt{2\alpha_j}$, velocities are v_j and initial phase constant are $x_{j,0}$, for $j=1,2$. Without loss of generality, we take $v_1=v/4$ and $v_2=-v/2$, so the approaching velocity of the two solitons is v. We also fix $\alpha_1=0.6$ and $\alpha_2=0.5$. The choices for the initial position parameters $x_{j,0}, j=1,2$, can be totally arbitrary. They will not affect the collision outcome as long as $x_{1,0}<0$ and $x_{2,0}>0$ are large enough. We fix $x_{1,0}=-x_{2,0}=10$ in our calculations.

In the first case, we choose $\beta=1$ and $v=0.5$. This is a Manakov model which is completely integrable and hence we expect the interaction of two solitons to be elastic and this is indeed the case (see Fig. 4). The computation is done for $0\leq t\leq 80$. The behaviors of solitons are completely known from exact inverse scattering solutions [1]. We observe that solitons collide at $t\approx 12$ and retain their identity after nonlinear interactions with the other soliton. The mass conservations I_1, I_2, the momentum conservation I_3 and the energy conservation E are also shown in Table 4. Although it seems that energy E almost keeps the same, while momentum I_3 varies because of the same reason as last example. Fig. 5 shows contours of Manakov type.

In the second test, we choose $\beta=0.3$ and $v=0.4$, which is inelastic collision between two orthogonally polarized solitons. The computation is done for $0\leq t\leq 70$. As mentioned in [28], the transmission, reflection and fusion scenarios depend on the precollision soliton parameters. Table 5 gives the conserved quantities which show exactly the same for I_1, I_2, the momentum conservation values I_3 varies because of collision and energy varies slightly after two solitons collision. Fig. 6 shows transmission wave of φ and ψ. Fig. 7 shows contours of two solitons fusion. We can see that there is fusion of two solitons into

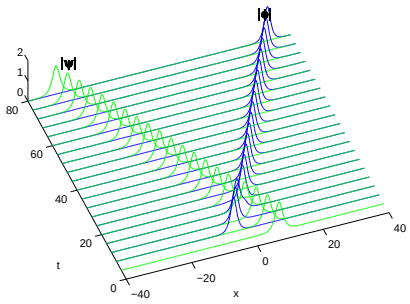

Figure 4: Interaction of two solitons (Manakov equation).

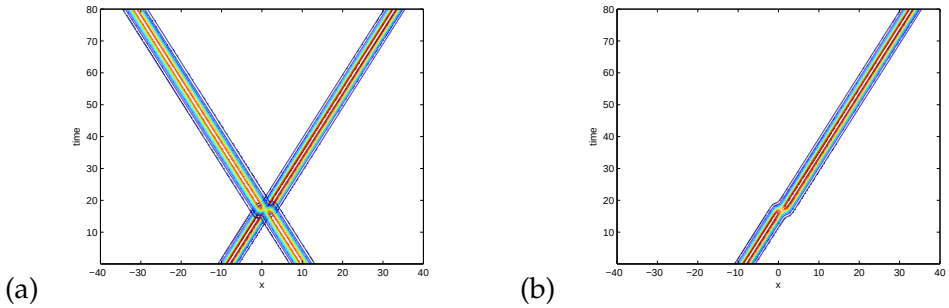

Figure 5: (a) Contours of Manakov type with $\beta=1$, $v=0.5$; (b) contour of φ for $\beta=1$, $v=0.5$.

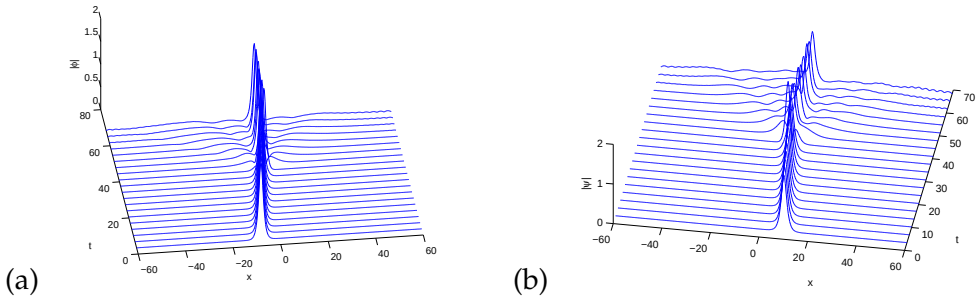

Figure 6: (a) Wave of φ for $\beta=0.3$, $v=0.4$; (b) wave of ψ for $\beta=0.3$, $v=0.4$.

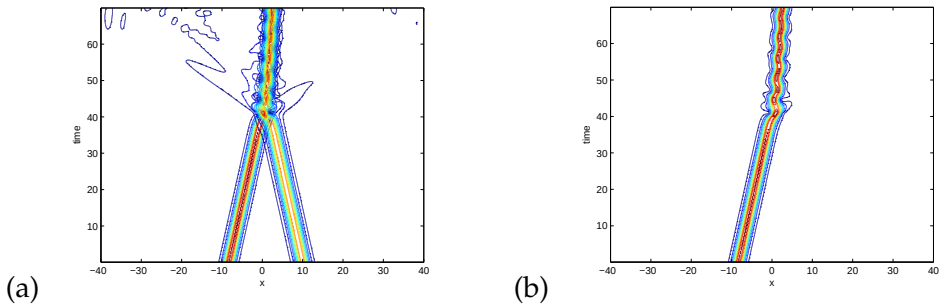

Figure 7: (a) Contours of two solitons fusion for $\beta=0.3$, $v=0.4$; (b) contour of φ for $\beta=0.3$, $v=0.4$.

Table 6: Conserved quantities ($\beta=2/3$, $v=0.4$).

Time	I_1	I_2	I_3	E	Iter. No.
0.0	9.59991459	7.99996509	-0.31992956	7.09842172	5
20.0	9.59991459	7.99996509	-0.31992956	7.09842252	5
40.0	9.59991459	7.99996509	-0.31610222	7.09842326	6
60.0	9.59991459	7.99996509	-0.31483488	7.09842354	6
80.0	9.59991459	7.99996509	-0.33704670	7.09842377	6

Table 7: Conserved quantities ($\beta=2/3$, $v=1.6$).

Time	I_1	I_2	I_3	E	Iter. No.
0.0	9.59987544	7.99994179	-1.27968893	4.45846614	6
20.0	9.59987544	7.99994179	-1.27824690	4.45846661	6
40.0	9.59987544	7.99994179	-0.93481861	4.45846688	6
60.0	9.59987544	7.99994179	-1.01186782	4.45846716	6
80.0	9.59987544	7.99994179	-1.07590965	4.45848456	6

one after the collision of the two solitons.

Next, we select $\beta=2/3$ and $v=0.4$, which gives the approaching velocity 0.4. For $\beta=2/3$, the CNLS equations represent real single-mode birefringent fibers, where φ and ψ represent the two-linear polarizations. Much theoretical and numerical work has been performed in [22,28]. Fig. 8 shows an interesting phenomenon. The right-moving soliton φ, which has larger momentum and energy, is reflected back by the collision. So it steadily decreases and becomes negative when it emerges from the collision. On the other hand, the left-moving soliton initially moves to the left but turns around after the collision. This reflection scenario has been reported in [29]. The amplitudes of the larger soliton gets even larger and the smaller one gets even smaller. These daughter waves are small pulses that split off from a solitary wave and propagate along beside it but in the other mode. From Fig. 9(a) we observe that the collision takes place at $t\approx 40$. Fig. 9(b) shows the contour of φ when $\beta=2/3$, $v=0.4$. In Table 6, we observe that the mass conservations have been kept, the energy changes slightly, while the momentum conservation varies from time to time because the collision takes place, but the total momentum conservation is conserved.

If we increase the colliding velocity v, we expect these two solitons to pass through each other. This is indeed the case. We repeat the test by increasing the velocity to $v=1.6$. We notice that, when the solitons come into collision, their velocities decrease significantly as before. We also notice that two waves pass through each other with some reshaping and radiation shedding and daughter waves are generated. This transmission scenario can be interpreted in Figs. 10 and 11. Table 7 shows the conserved quantities with $\beta=2/3$ and $v=1.6$. The mass conservations keep the same, the energy conservation keeps almost the same, while the single momentum conservation changes over time because of collision of solitons, the total momentum quantities keep the same.

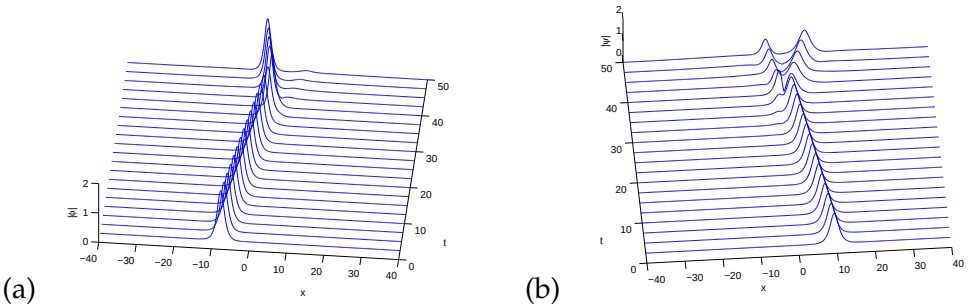

(a) (b)

Figure 8: (a) Wave of φ for $\beta=2/3$, $v=0.4$; (b) wave of ψ for $\beta=2/3$, $v=0.4$.

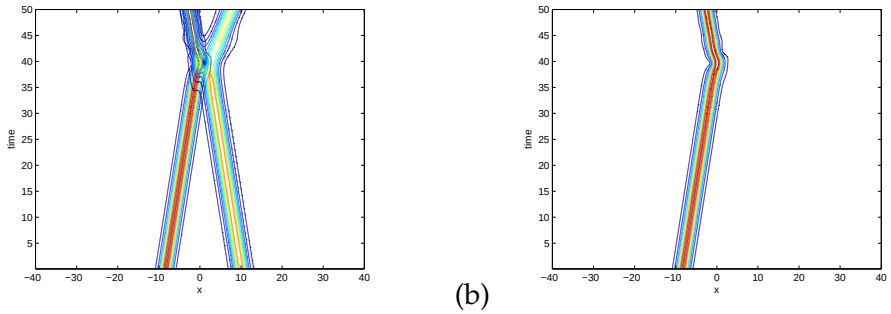

(a) (b)

Figure 9: (a) Contours of two interaction for $\beta=2/3$, $v=0.4$; (b) contour of φ for $\beta=2/3$, $v=0.4$.

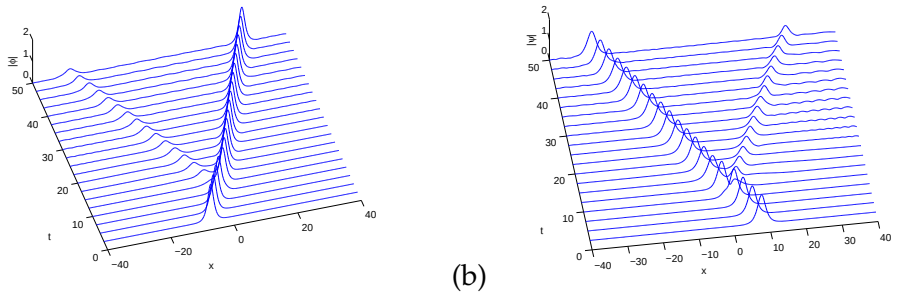

(a) (b)

Figure 10: (a) Wave of φ for $\beta=2/3$, $v=1.6$; (b) wave of ψ for $\beta=2/3$, $v=1.6$.

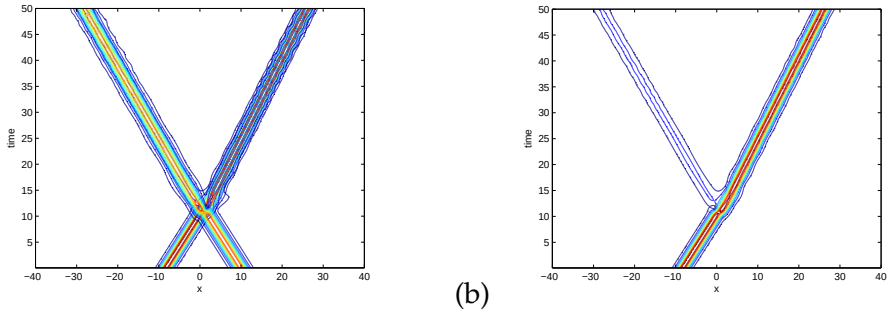

(a) (b)

Figure 11: (a) Contours of two interaction for $\beta=2/3$, $v=1.6$; (b) contour of φ for $\beta=2/3$, $v=1.6$.

The last test concerning the creation of new vector solitons which can be happened when β is large and positive. As expected, after interaction, these two solitary waves are significantly reshaped; large daughter waves are created; and radiation is also shedded. A novel feature is that new solitary waves are created. These new waves travel at speeds very different from those of the original two solitary waves. One example with $\beta=4$ and $v=1.6$ is shown in Fig. 12, four new solitary waves are generated for wave φ and ψ. Fig. 13 gives contour of creation scenario with $\beta=2$ and $v=1.6$; and $\beta=3$ and $v=1.6$, respectively. We observe that two and three new solitary waves are created.

5.4 Periodic boundary conditions

We consider the periodic boundary conditions (2.12). In the test we select the parameters

$$\begin{aligned} &x_L=-40, \quad && x_R=40, \quad && \alpha_1=0.6, \quad && \alpha_2=0.5, \\ &\beta=0.3, && v_1=0.15, && v_2=-0.6, && x_{1,0}=-x_{2,0}=10. \end{aligned}$$

The computation is done for $0\leq t\leq 80$. The interaction scenario is given in Fig. 14(a), Fig. 14(b) shows contours of the interaction scenario. The two waves interact at $t=20$ and $t=75$ and leave the interaction without any change in behavior shape and velocity. The numerical results show that the soliton moves to the left periodically, it disappears at $x=x_L$, but reappears at $x=x_R$. Table 8 gives the conserved quantities which show exactly the same. It is clear that all of these quantities are recovered after the interaction.

Table 8: Conserved quantities with periodic boundary conditions.

Time	I_1	I_2	I_3	E	Iter. No.
0.0	4.79999666	3.99998777	3.35997108	-0.63866341	4
20.0	4.79999666	3.99998777	3.35996743	-0.63866341	4
40.0	4.79999666	3.99998777	3.35998267	-0.63866341	4
60.0	4.79999666	3.99998777	3.35997229	-0.63866341	4
80.0	4.79999666	3.99998777	3.35994856	-0.63866341	4

6 Conclusions

We have developed the OSC method to solve coupled nonlinear Schrödinger equations. We use finite difference for time discretization, while the OSC method is used for space discretization. The stability and convergence of solutions with order $\mathcal{O}(h^4+\tau^2)$ are also proved in the energy norm. We observe that the scheme simulates the evolution of the solitons and preserves conserved quantities well. It has advantage for the long time computing accuracy and preserving the conservation properties. The algorithm is relatively simple and has been shown to handle easily. The derived method can be easily generalized to solve N coupled Schrödinger equations. And this method is applicable for the

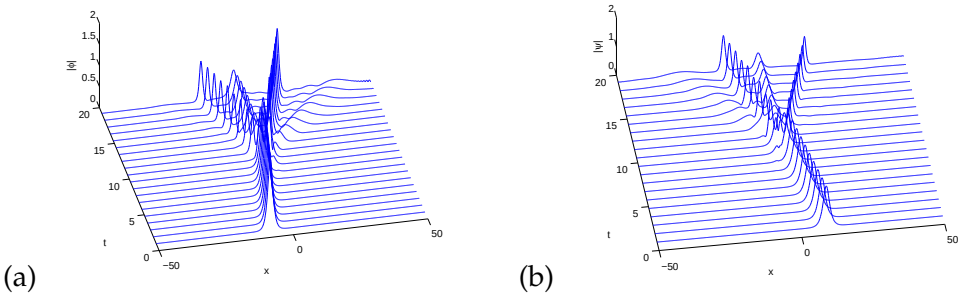

Figure 12: (a) Wave of φ for $\beta=4$, $v=1.6$; (b) wave of ψ for $\beta=4$, $v=1.6$.

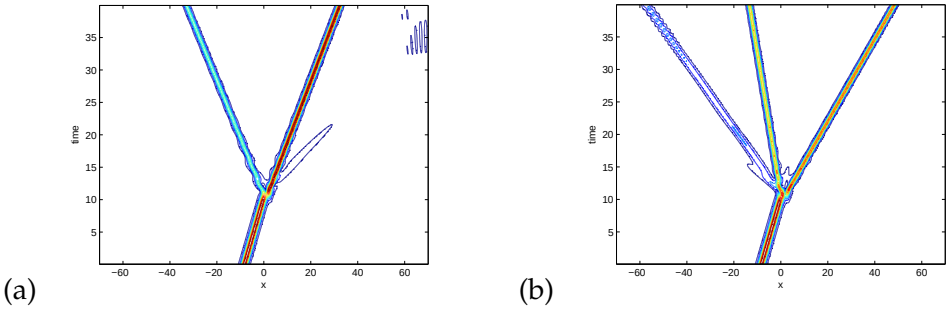

Figure 13: (a) Contours of φ for $\beta=2$; (b) contours of φ for $\beta=3$.

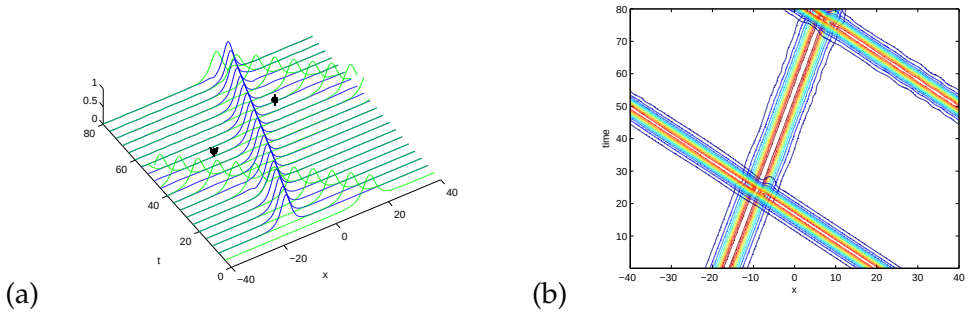

Figure 14: (a) Interaction of two solitons with periodic boundary conditions; (b) contours of two solitons with periodic boundary conditions.

study of the dynamics of a broad spectrum of complex physical and engineering problems.

Acknowledgments

The first and the third authors gratefully acknowledge the support of UL020/08-Y4/MAT/-JXQ01/FST from University of Macau. The second and the fourth authors

acknowledge the support of the Key National Natural Science Foundation of China under contract 40730842. The authors are very grateful to the anonymous referees for their valuable comments and suggestions which have improved the paper. The authors are also very much thankful to the editor, Professor Tao Tang.

References

[1] M. J. Ablowitz and H. Segur, Solitons and the Inverse Scattering Transform, SIAM, Philadelphia, 1981.
[2] X. Antoine, A. Arnold, C. Besse, M. Ehrhardt and A. Schädle, A review of transparent and artificial boundary conditions techniques for linear and nonlinear Schrödinger equations, Commun. Comput. Phys., 4 (2008), 729–796.
[3] W. Z. Bao, Ground states and dynamics of multicomponent Bose-Einstein condensates, Multiscale Model. Simul., 2 (2004), 201–236.
[4] W. Z. Bao and J. Shen, A fourth-order time-splitting Laguerre-Hermite pseudospectral method for Bose-Einstein condensates, SIAM J. Sci. Comput., 26 (2005), 2010–2028.
[5] W. Z. Bao and C. X. Zheng, A time-splitting spectral method for three-wave interactions in media with competing quadratic and cubic nonlinearities, Commun. Comput. Phys., 2 (2007), 123–140.
[6] D. J. Benney and A. C. Newell, Random wave closures, Stud. Appl. Math., 48 (1969), 29–53.
[7] C. de Boor and B. Swartz, Collocation at Gauss points, SIAM. J. Numer. Anal., 10 (1973), 582–606.
[8] Q. S. Chang, E. H. Jia and W. W. Sun, Difference schemes for solving the generalized nonlinear Schrödinger equation, J. Comput. Phys., 148 (1999), 397–415.
[9] Y. M. Chen, H. J. Zhu and S. H. Song, Multi-symplectic splitting method for the coupled nonlinear Schrödinger equation, Comput. Phys. Commun., 181 (2010), 1231–1241.
[10] J. Douglas Jr and T. Dupont, Collocation Methods for Parabolic Equations in a Single Space Variable, Lecture Notes in Math, Vol. 385, Spring-Verleg, New York, 1974.
[11] G. Fairweather and D. Meade, A survey of spline collocation methods for the numerical solution of differential equations, in: J. C. Diaz ed., Mathematics for Large Scale Computing, Lecture Notes in Pure Appl. Math., Vol. 120, Marcel Dekker, New York, (1989), 297–341.
[12] B. Y. Guo, J. P. Pedro, J. R. Maria and V. Luis, Numerical solution of the Sine-Gordon equation, Appl. Math. Comput., 18 (1986), 1–14.
[13] M. S. Ismail and S. Z. Alamri, Highly accurate finite difference method for coupled nonlinear Schrödinger equation, Int. J. Comput. Math., 81 (2004), 333–351.
[14] M. S. Ismail and T. R. Taha, Numerical simulation of coupled nonlinear Schrödinger equation, Math. Comput. Simul., 56 (2001), 547–562.
[15] P. Klein, X. Antoine, C. Besse and M. Ehrhardt, Absorbing boundary conditions for solving N-dimensional stationary Schrödinger equations with unbounded potentials and nonlinearities, Commun. Comput. Phys., 10 (2011), 1280–1304.
[16] C. R. Menyuk, Nonlinear pulse propagation in birefringent optical fibers, IEEE J. Quantum Electron., 23 (1987), 174–176.
[17] M. P. Robinson and G. Fairweather, Orthogonal spline collocation methods for Schrödinger-type equations in one space variable, Numer. Math., 68 (1994), 355–376.
[18] J. Q. Sun, X. Y. Gu and Z. Q. Ma, Numerical study for the soliton waves of the coupled nonlinear Schrödinger system, Phys. D, 196 (2004), 311–328.

[19] J. Q. Sun and M. Z. Qin, Multi-symplectic methods for the coupled 1D nonlinear Schrödinger system, Comput. Phys. Commun., 155 (2003), 221–235.
[20] M. Thalhammer, M. Caliari and C. Neuhauser, High-order time-splitting Hermite and Fourier spectral methods, J. Comput. Phys., 228 (2009), 822–832.
[21] T. Utsumi, T. Aoki, J. Koga and M. Yamagiwa, Solutions of the 1D coupled nonlinear schrödinger equations by the CIP-BS method, Commun. Comput. Phys., 1 (2006), 261–275.
[22] T. Ueda and W. L. Kath, Dynamics of coupled solitons in nonlinear optical fibers, Phys. Rev. A, 42 (1990), 563–571.
[23] H. Q. Wang, Numerical studies on the split step finite difference method for the nonlinear Schrödinger equations, Appl. Math. Comput., 170 (2005), 17–35.
[24] M. Wadati, T. Izuka and M. Hisakado, A coupled nonlinear Schrodinger equation and optical solitons, J. Phys. Soc. Jpn., 61 (1992), 2241–2245.
[25] Y. Xu and C. W. Shu, Local discontinuous Galerkin methods for nonlinear Schrödinger equations, J. Comput. Phys., 205 (2005), 72–97.
[26] Y. Xu and C. W. Shu, Local discontinuous Galerkin methods for high-order time-dependent partial differential equations, Commun. Comput. Phys., 7 (2010), 1–46.
[27] Y. Xu and C. W. Shu, Local discontinuous Galerkin methods for the Degasperis-Procesi equation, Commun. Comput. Phys., 10 (2011), 474–508.
[28] J. K. Yang, Multisoliton perturbation theory for the Manakov equations and its applications to nonlinear optics, Phys. Rev. E, 59 (1999), 2393–2405.
[29] J. K. Yang and D. J. Benney, Some properties of nonlinear wave systems, Stud. Appl. Math., 96 (1996), 111–135.
[30] Y. Z. Zhang, W. Z. Bao and H. L. Li, Dynamics of rotating two-component Bose-Einstein condensates and its efficient computation, Phys. D, 234 (2007), 49–69.